This article has been accepted for publication in IEEE Transactions on Applied Superconductivity. This is the author's version which has not been fully edited and content may change prior to final publication. Citation information: DOI 10.1109/TASC.2023.3241833

An initial look at the magnetic design of a 150 mm aperture high-temperature superconducting magnet with a dipole field of 8 to 10 T

X. Wang, D. Arbelaez, L. Brouwer, S. Caspi, P. Ferracin, L. Garcia Fajardo, S. Gourlay, H. Higley, M. Juchno, M. Marchevsky, I. Pong, S. Prestemon, J. L. Rudeiros Fernandez, G.L. Sabbi, T. Shen, R. Teyber, G. Vallone, D. van der Laan, J. Weiss

***Abstract*—High-temperature superconducting $REBa_2Cu_3O_{7-x}$ (REBCO) conductors have the potential to generate a high magnetic field over a broad temperature range. The corresponding accelerator magnet technology, still in its infancy, can be attractive for future energy-frontier particle colliders such as a multi-TeV muon collider. To help develop the technology, we explore the requirements and potential characteristics of a REBCO magnet, operating at 4.2 or 20 K, with a dipole field of 8 -- 10 T in a clear aperture of 150 mm. We use the canted $\cos\theta$ magnet configuration to reduce the electromagnetic stresses on the conductors. We present the resulting dipole fields, field gradients for combined-function cases, conductor stresses, magnet dimensions and conductor lengths. We also discuss the conductor performance that is required to achieve the target dipole field at 4.2 and 20 K. The information can provide useful input to the development of REBCO magnet and conductor technology for collider-ring magnets in a muon collider.**

***Index Terms*—REBCO, muon collider, arc magnet**

I. Introduction

HIGH-field accelerator magnets enable future energy-frontier colliders [1], such as a multi-TeV muon collider that offers enormous potential for particle physics but is also challenging to build [2]–[6].

To generate a dipole field above 16 T, a practical limit of today's Nb_3Sn conductors, the magnet community is taking several approaches to develop magnet technology using high-temperature superconductors (HTS), such as $Bi_2Sr_2CaCu_2O_{8-x}$ and $REBa_2Cu_3O_x$ (RE = rare earth, REBCO) [1]. One approach focuses on the HTS/Nb_3Sn hybrid configuration [7], [8]. This approach effectively leverages conductor grading, as it replaces the otherwise HTS outer coils with Nb_3Sn coils that are relatively less expensive than HTS [9].

Manuscript received December 4, 2022. This work was supported by the U.S. Magnet Development Program through Director, Office of Science, Office of High Energy Physics of the US Department of Energy under contracts DE-AC02-05CH11231.

X. Wang, D. Arbelaez, L. Brouwer, S. Caspi, P. Ferracin, L. Garcia Fajardo, H. Higley, M. Juchno, M. Marchevksy, I. Pong, S. Prestemon, J. L. Rudeiros Fernandez, G.L. Sabbi, T. Shen, R. Teyber, G. Vallone are with Lawrence Berkeley National Laboratory, Berkeley, CA 94720. (e-mail: xrwang@lbl.gov).

S. Gourlay is with Fermi National Accelerator Laboratory, Batavia, IL 60510. (e-mail:sgourlay@fnal.gov).

D. van der Laan and J. Weiss are with Advanced Conductor Technologies, LLC, Boulder, CO 80301 and the University of Colorado, Boulder, CO 80309.

Another approach uses only high-temperature superconductors. The all-HTS approach is unavoidable as we are destined for higher fields [10], [11]. Moreover, high-temperature superconducting magnets can operate at elevated temperatures, especially for REBCO, our focus here [12].

Higher operating temperatures improve cooling efficiency and reduce power consumption of large cryogenics systems. Studies at the Large Hadron Collider show that the coefficient of cooling performance improves by a factor of 3.5 from 1.9 to 4.5 K and by a factor of 10 from 1.9 to 20 K based on the Carnot factor [13], [14]. The improved cooling efficiency makes future colliders more affordable and sustainable because the cryogenics system for the superconducting magnets is a key power consumer [15]–[17].

HTS accelerator magnets operating at elevated temperatures can also help address the heat-load and radiation-damage challenges that can be unprecedented in a muon collider [18]–[20].

Finally, an elevated operating temperature allows cooling options beyond liquid helium, the essential coolant for superconducting accelerator magnets that has become scarce in recent years [21].

Despite its potential, REBCO accelerator magnet technology is in its infancy, with slowly evolving conductor architectures and magnet concepts. The European programs have demonstrated a dipole field of 5.4 T in a racetrack design and 4.5 T in a dipole magnet with a 40 mm aperture, both at 4.2 K [22]–[24]. The latter also demonstrated successful operation from 85 to 5 K with increased field generation [23]. The U.S. Magnet Development Program, in collaboration with conductor vendors, is working to generate a dipole field of 5 T [25]–[29].

Meanwhile, the fusion community is developing REBCO magnets for high-field compact fusion reactors that can affect the future circular colliders in multiple ways [30]–[34].

In this context, we started a design study of a REBCO magnet that can generate a dipole field of 8 – 10 T, a stretch goal beyond 5 T, also to keep engaging conductor vendors.

Such a field range is relevant for a muon collider with a center-of-mass energy of 3 TeV [35]. Although the maturing Nb_3Sn magnet technology can cover this field range [36]–[40], developing a REBCO version is a critical practice and stepping stone to meet the needs of future colliders.

This article has been accepted for publication in IEEE Transactions on Applied Superconductivity. This is the author's version which has not been fully edited and content may change prior to final publication. Citation information: DOI 10.1109/TASC.2023.3241833

We report the results of an initial conceptual study of a large-aperture REBCO dipole magnet using CORC® wires for the storage ring of a muon collider. The design is based on the canted $\cos\theta$ (CCT) concept. Our driving questions are:

- Based on the demonstrated performance of CORC® conductors, what magnet performance can we expect at 4.2 and 20 K?
- How much conductor do we need to make such a magnet?
- What further magnet and conductor development is needed?

By addressing these questions, we hope to eventually achieve two goals with the broader community: 1) to provide feedback to the development of REBCO high-field magnets; 2) to plant a seed towards an affordable and sustainable multi-TeV muon collider.

II. Properties of Existing CORC® Conductors

CORC® wires, developed and commercialized by Advanced Conductor Technologies LLC, consist of multiple REBCO tapes helically wrapped around a metal core [41], [42]. Although not fully transposed, the resulting wire is mechanically and electromagnetically isotropic, convenient to design and make magnets.

One may adjust the bending and current-carrying capability of a CORC® wire in two ways: the number and property of REBCO tapes; and the wire fabrication process.

We use the performance of CORC®-02, a prototype CORC® wire made of commercial REBCO tapes [43], as a starting point to determine the magnet performance. The wire has 32 tapes distributed in 16 layers around a Cu former. The wire diameter is 3.4 mm.

The critical current of CORC®-02 wire was measured at a bend radius of 31.5 mm and 4.2 K, as a function of applied magnetic flux density, B, ranging from 8 to 12 T. The applied magnetic field is transverse to the CORC® wire. The measured critical current follows a power law of

$$I_c(B) = \beta B^{\alpha}, \tag{1}$$

where β is a constant and $\alpha = -0.77$ [43].

The existing data show that the critical current of commercial REBCO tapes decreases by about 50% when the operating temperature increases from 4.2 to 20 K, with the applied magnetic field perpendicular to the tape broad surface [44]–[46]. We assume that the critical current of a CORC® wire follows the same temperature dependence. We choose 20 K, considering liquid H_2 as a potential coolant for REBCO magnets [47].

The wire shows no degradation in critical current under cycling $\mathbf{I} \times \mathbf{B}$ electromagnetic forces up to 50 kN m^{-1} at 4.2 K [43].

We use 30 mm as the minimum bend radius for the CORC® conductors.

III. Conceptual CCT Magnets for the Storage Ring of a Muon Collider

The CCT concept [48]–[53] offers several attractive features for a large-aperture accelerator magnet. A CCT magnet can effectively intercept the accumulation of electromagnetic stresses on the conductors that are embedded in the magnet mandrels. This can help address the high electromagnetic stresses on conductors resulting from a combination of high dipole field and large magnet aperture as required by a muon collider. The design also offers excellent geometric field quality. The magnet performance can be analytically determined [53]–[55], useful for design studies.

We consider two magnet cases for the storage ring in a muon collider with a center-of-mass energy of 3 TeV. First, a dipole magnet to set a baseline for the magnet performance and parameters. Second, a dipole-quadrupole combined-function magnet to avoid the neutrino hot spot [2], [18].

The dipole case has two designs, one with four nested layers and the other with six nested layers. The combined-function case has six nested layers. Each design has three cases: with one, two, or three CORC® wires in the groove. The wires form a ribbon-type cable, electrically parallel without transposition.

Table I lists the main geometric parameters for the conceptual CCT magnets. Groove depth and therefore layer thickness varies according to the number of wires in the groove.

TABLE I
Main Geometric Parameters for the Conceptual CCT Magnets.

Parameter	Unit	Value
Clear aperture	mm	150
Spar thickness	mm	5
Groove diameter	mm	4.1
Rib thickness at the mid-plane	mm	0.5
Radial clearance between Layers	mm	1
Number of layers	–	4 or 6

A. Dipole case

Suppose the longitudinal axis of the CORC® wire follows a space curve $\mathbf{C}(t) = (x(t), y(t), z(t))$ in a Cartesian coordinate system with the parameter t. For the single CORC® wire at the bottom of the groove, we have

$$\mathbf{C}(t) = \left(r\cos t, r\sin t, \frac{r\sin t}{\tan\theta} + p\,t \right), \tag{2}$$

where r is the radius of the wire axis, when projected to the x-y plane, and $2\pi p$ gives the wire pitch along the z axis. We define the wire tilt angle as the angle between the wire axis, when projected to the y-z plane, and the z axis, at $t = 0$ [53] (Fig. 1).

For the four-layer design, the tilt angle is θ for the pure multi-pole magnet case. The tilt angle is 22° in Layers 1 and 2, and 18° in Layers 3 and 4. The tilt angle is 16° in Layers 5 and 6 for the six-layer design.

When the groove contains a single stack of wires, if Wire 1 at the bottom of the groove follows (2) with r_1 and θ_1, then we have $\tan\theta_n / \tan\theta_1 = r_n / r_1$ for Wire n [29], [55].

Fig. 1 shows two CCT layers for a dipole case with ten turns of a single CORC® wire.

Based on the conductor peak field and the conductor $I_c(B)$ from (1), we determine the maximum dipole field, or the short-sample prediction, for various designs. At 4.2 and 20 K, the

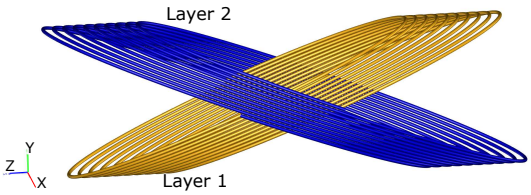

Fig. 1. Layer 1, gold and Layer 2, blue, of a dipole design. Only ten turns of a single CORC® wire are shown.

current-carrying capability of a REBCO tape is usually limited by the field perpendicular to the tape broad surface [56]. Therefore, we use the field component that is transverse to the longitudinal axis of the CORC® wire to determine the conductor peak field. Fig. 2 shows an example of the load line for a six-layer three-wire design.

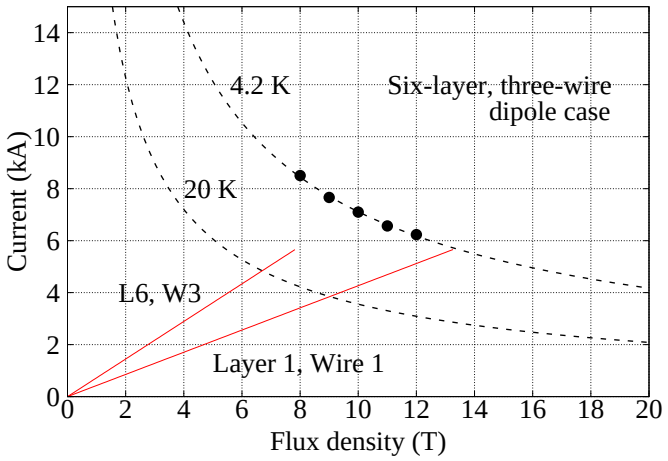

Fig. 2. Load line for the peak conductor field on Layer 1, Wire 1 for the dipole design with six layers and three wires (red solid line), without iron. The conductor-field load line for Layer 6, Wire 3 is also included. The top black dashed line is the power-law fit of the measured $I_c(B)$ data at 4.2 K from [43] (circles). The bottom dashed line is an imagined $I_c(B)$ data for the same conductor at 20 K, assuming 50% reduction in I_c from 4.2 K for the same applied flux density.

Table II lists the short-sample prediction of the dipole field of the various designs, without iron. The dipole-field transfer function (TF) is defined as the ratio between the dipole field in the magnet aperture and the total magnet current. The magnet inductance is estimated by approximating the ribbon-type cable as a line current located at the geometric center of the cable [53]. B_p in Table II is the peak field transverse to the longitudinal axis of the wire. The inductance L, stored energy E, and conductor length l are for a unit magnetic length. R_{min} is the minimum bend radius of the wire. OD is the magnet outer diameter without iron.

The total tape length scales from the total CORC® wire length by a ratio of 57. Two factors determine the ratio: the number of tapes in a CORC® wire, 32 for CORC®-02 wire [43], and the length reduction when a tape transforms from a straight to helical shape.

We calculate the eletromagnetic force, based on $\mathbf{J} \times \mathbf{B}$, on the wire to assess if the wire can sustain the magnetic force during operation. The force is transverse to the longitudinal

TABLE II
SHORT-SAMPLE PREDICTION OF THE DIPOLE FIELD B_1 AND MAIN CHARACTERISTICS OF VARIOUS DESIGNS AT 4.2 AND 20 K, WITHOUT IRON.

Number of layers		4			6		
Number of wires per layer		1	2	3	1	2	3
TF	T kA^{-1}	0.52	0.51	0.51	0.79	0.78	0.77
$B_p/B_1 - 1$	%	5	2.4	0.5	2.2	0.4	0.2
L	mH m^{-1}	11	12	13	30	34	40
R_{min}	mm			30			
OD	mm	229	262	294	270	319	368
B_1(4.2 K)	T	5.6	8.3	10.5	7.2	10.6	13.2
I_{total}(4.2 K)	kA	10.7	16.1	20.5	9.0	13.6	17.2
E(4.2 K)	MJ m^{-1}	0.6	1.6	2.8	1.2	3.1	5.8
B_1(20 K)	T	3.8	5.6	7.1	4.8	7.2	8.9
I_{total}(20 K)	kA	7.2	10.9	13.9	6.1	9.2	11.6
E(20 K)	MJ m^{-1}	0.3	0.7	1.3	0.6	1.4	2.6
l_{wire}	km m^{-1}	0.4	0.9	1.4	0.7	1.4	2.3
l_{tape}	km m^{-1}	23	51	80	40	80	131

axis of the wire because the current density vector $\mathbf{J}$ is tangent to the longitudinal axis of the wire.

The six-layer three-wire design sets the upper bound of the electromagnetic force on the CORC® wire of all the designs in Table II. The peak force density is about 110 mN mm^{-3} at 1 kA (Fig. 3). The corresponding peak electromagnetic force on the wire, at the short-sample prediction, is 33 kN m^{-1} at 4.2 K and 15 kN m^{-1} at 20 K. Assuming a 1 mm contact width between the wire and mandrel, the peak force density translates to about 33 MPa stress transverse to the CORC® wire.

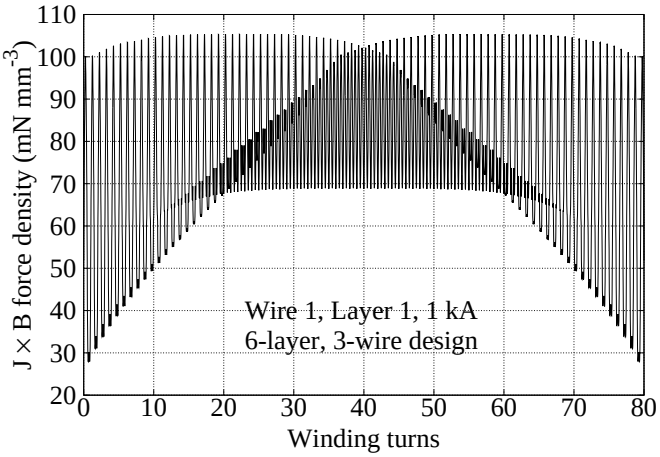

Fig. 3. The distribution of the electromagnetic force density at 1 kA along Layer 1 Wire 1 in the six-layer three-wire design.

Table III gives the normal terms of the integrated geometric field errors of the six-layer three-wire dipole design, calculated by the Opera 3D software. The integrated field errors are defined as

$$\bar{b}_n + i\,\bar{a}_n = \frac{\int [B_n(z) + i\,A_n(z)]dz}{\int B_1(z)dz} 10^4, \qquad (3)$$

where B_n is the normal and A_n is the skew multipole of

This article has been accepted for publication in IEEE Transactions on Applied Superconductivity. This is the author's version which has not been fully edited and content may change prior to final publication. Citation information: DOI 10.1109/TASC.2023.3241833

order n. B_1 is the main dipole field. The multipoles vary along the z-axis, the longitudinal axis of the magnet (Fig. 1). The field errors are in units of 10^{-4} of the main dipole field, at a reference radius of 50 mm. The skew terms are practically zero.

TABLE III
INTEGRATED GEOMETRIC FIELD ERRORS OF THE SIX-LAYER THREE-WIRE CCT DIPOLE, WITHOUT IRON. UNIT: 10^{-4} OF THE MAIN DIPOLE FIELD.

$\bar{b}_2$	$\bar{b}_3$	$\bar{b}_4$	$\bar{b}_5$	$\bar{b}_6$	$\bar{b}_7$	$\bar{b}_8$	$\bar{b}_9$
0.00	−0.02	0.00	0.00	0.00	0.00	0.00	0.00

B. Dipole-quadrupole combined-function case

A combined-function magnet can take at least two configurations. One is through asymmetric conductor placement [39], [57], [58]. The other is a nested configuration with a dipole coil inside a quadrupole coil or vice versa [38], [39]. The CCT concept can work with either configuration [53], [59], [60]. We start with the first approach to save conductors.

For a single layer of combined-function CCT coil, the longitudinal axis of a CORC® wire follows

$$\mathbf{C}(t) = \left(r\cos t,\, r\sin t,\, \eta\,\frac{r\sin t}{\tan\theta} + \varepsilon\,\frac{r\sin 2t}{2\tan\theta} + p\,t \right), \quad (4)$$

where η scales the dipole field and ε scales the quadrupole field. Although the definition for the tilt angle for the combined-function case remains the same as in the dipole case (Section III-A), its value deviates from θ in (4). Using the small-angle approximation, we find the actual tilt angle θ' as

$$\theta' = \arctan\left(\frac{\tan\theta}{\eta+\varepsilon}\right). \quad (5)$$

Fig. 4 shows two CCT layers for a combined-function design with ten turns of a single CORC® wire.

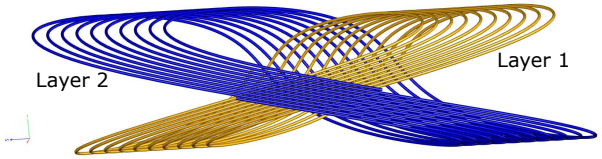

Fig. 4. Layer 1, gold and Layer 2, blue, of the combined-function design. Only ten turns of a single CORC® wire are shown.

The transfer functions of the dipole and quadrupole fields depend on the scaling factors η and ε. Here we consider a case with $\eta = 1$ and $\varepsilon > 0$. As ε increases, we gain on the quadrupole component and lose on the dipole component as the tilt angle θ' decreases and the pitch length increases, consistent with earlier findings [59].

We use the six-layer three-wire design from Table II as the basis to introduce the quadrupole component. We vary ε from 0.5 to 0.9 to maintain a dipole field of around 8 T at 4.2 K, which can allow a comparison with the Nb_3Sn magnet design and technology [38]. Table IV gives the short-sample prediction of the resulting combined-function magnets. The inductance L, stored energy E, and conductor length l in Table IV are again for a unit magnetic length.

TABLE IV
SHORT-SAMPLE PREDICTION OF THE COMBINED-FUNCTION MAGNETS WITH DIFFERENT GRADIENTS, WITHOUT IRON.

	$\varepsilon(\eta=1)$	0.5	0.7	0.9
$\theta_{1,2}$	degree	33	39	44
$\theta_{3,4}$	degree	24	28	33
$\theta_{5,6}$	degree	20	24	28
$R_{\min}$	mm		30	
B_1 TF	T kA^{-1}	0.51	0.45	0.40
G TF	T m^{-1} kA^{-1}	2.00	2.45	2.80
L	mH m^{-1}	20	16	14
B_1(4.2 K)	T	9.7	8.6	7.7
G(4.2 K)	T m^{-1}	37.9	46.7	53.8
$B_{\rm p}$(4.2 K)	T	11.7	11.5	11.4
$I_{\rm total}$(4.2 K)	kA	18.9	19.1	19.3
E(4.2 K)	MJ m^{-1}	3.5	3.0	2.7
B_1(20 K)	T	6.5	5.8	5.2
G(20 K)	T m^{-1}	25.6	31.7	36.4
$B_{\rm p}$(20 K)	T	7.9	7.8	7.7
$I_{\rm total}$(20 K)	kA	12.8	12.9	13.0
E(20 K)	MJ m^{-1}	1.6	1.4	1.2
$l_{\rm wire}$	km m^{-1}	1.9	1.8	1.8
$l_{\rm tape}$	km m^{-1}	108	103	103

The θ value for each layer increases from that in the dipole case to keep the minimum bend radius of the wire at 30 mm. Otherwise, the minimum bend radius is 20 mm for ε of 0.5 and is 13 mm for ε of 0.9. The increased tilt angle, however, only reduces the short-sample prediction by less than 6% from the case with the original θ value.

In all three cases of Table IV, the transverse force density on a single CORC® wire is less than 110 mN mm^{-3} at 1 kA, similar to the six-layer three-wire dipole case. This translates to a peak force of 41 kN m^{-1} on a single wire at the short-sample limit, 4.2 K.

Table V gives the integrated, normal, geometric field errors of the combined-function magnets. The reference radius is 50 mm. The skew terms are less than 0.01 units.

TABLE V
INTEGRATED GEOMETRIC FIELD ERRORS OF THE COMBINED-FUNCTION DESIGN, WITHOUT IRON. UNIT: 10^{-4} OF THE MAIN DIPOLE FIELD. $\eta = 1$.

ε	$\bar{b}_2$	$\bar{b}_3$	$\bar{b}_4$	$\bar{b}_5$	$\bar{b}_6$	$\bar{b}_7$	$\bar{b}_8$	$\bar{b}_9$
0.5	1895	0.02	−0.02	−0.01	0.00	0.00	0.00	0.00
0.7	2648	0.05	−0.03	−0.01	0.00	0.00	0.00	0.00
0.9	3405	0.07	−0.03	−0.01	−0.01	0.01	0.00	0.00

Fig. 5 shows the vectors of flux density on the $z = 0$ plane for the dipole and combined-function cases.

IV. DISCUSSION

Based on the performance of the existing CORC® wire, we can generate the target dipole field of 8 – 10 T at 4.2 K using four CCT layers and a ribbon-type cable of two or three wires in each layer. The dipole field decreases by about 33% when the operating temperature increases from 4.2 to 20 K (Table II). This is due to the reduction of the conductor

This article has been accepted for publication in IEEE Transactions on Applied Superconductivity. This is the author's version which has not been fully edited and content may change prior to final publication. Citation information: DOI 10.1109/TASC.2023.3241833

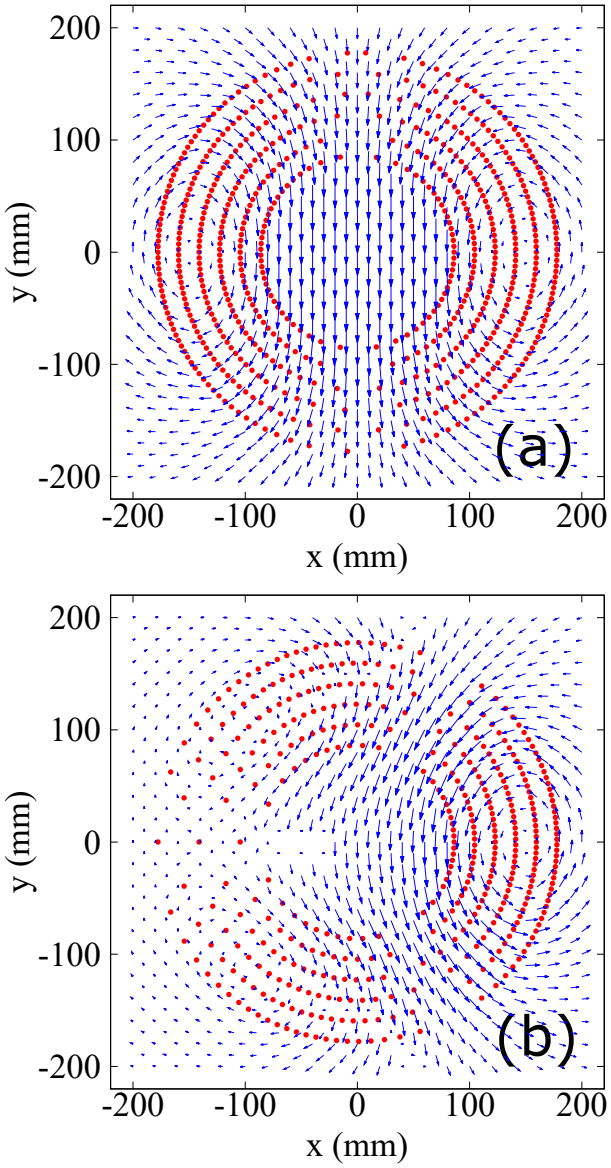

Fig. 5. Vectors of flux density on the $z = 0$ plane for (a) the dipole case and (b) the combined-function case. Both cases have six layers and three wires in each layer. The red dots represent the centers of Wire 2 in each layer when the wires cross the $z = 0$ plane.

critical current, as explained in Appendix A. We need the six-layer three-wire design to generate 8 T at 20 K using today's conductor (Table II).

The performance of the combined-function cases at 4.2 K can also meet the target dipole field range of 8 – 9 T, although the gradient up to about 50 T m^{-1} is lower than the maximum target gradient of 87 T m^{-1} [35]. The 50 T m^{-1} gradient is also lower than the 80 T m^{-1} level that can be achieved by the nested design for Nb_3Sn [38]. Thicker coils with more CCT layers or a nested version should be studied. The maximum dipole field and gradient reduce by 33% from 4.2 to 20 K (Table IV).

Although a ribbon-type cable using CORC® wires is a straightforward option to increase the total magnet current and magnetic fields, there can be issues. The electrical resistance at the cable terminations will affect the current distribution among the wires. The current distribution may not be uniform during current ramping as the wires are not transposed.

A higher conductor critical current is necessary to reduce the number of wires in a ribbon-type cable or eliminate it. Suppose we use only one wire in each layer for the designs in Table II, we may use (7) to estimate the necessary conductor I_c for design cases without iron.

For instance, if we double the I_c of CORC®-02, from 6 to 12 kA at 12 T 4.2 K (Fig. 2), then the short-sample prediction will increase to 8.4 T for the four-layer design and 10.8 T for the six-layer design, both at 4.2 K. This corresponds to a whole-wire current density of about 1000 A mm^{-2} at 12 T, 4.2 K. If we triple the I_c of CORC®-02 for the same applied flux density, the six-layer single-wire design will generate around 9 T at 20 K.

To reach the ambitious I_c target, we need to continue increasing the critical current in REBCO tape over a temperature range from 4.2 to 20 K. Including more tapes in a wire is also viable to increase the I_c of CORC® wires [61]; maintaining the wire bend radius around 30 mm or less requires a system approach to optimize the tape geometry and cable fabrication process. Therefore, it is critical to continue engaging and collaborating with conductor vendors to address our magnet needs.

We expect the CORC® wire to survive the electromagnetic force as the wire demonstrated no degradation after cycling to 50 kN m^{-1} at 4.2 K [43]. The expected transverse stress is also below the 100 MPa stress limit where the conductor degradation occurs under an applied load, without epoxy impregnation [62]. The analysis reported here does not consider the tensile load on the CORC® wire that appears in the CCT configuration. Detailed analysis on the mechanics of conductor and magnet structures with more realistic conditions will be carried out in future studies [63], [64]. More experimental data on the conductor performance under transverse electromagnetic forces are important to inform future magnet and conductor designs aiming at a dipole field of 15 T or higher.

The results presented here are determined without iron. Actual magnets will need iron to reduce the fringe field. We estimate a roughly 500 mm thick iron for a dipole field of 13 T and an aperture of 150 mm [65]. The six-layer three-wire magnet in Table II would have an OD of 1.4 m with the iron. The iron yoke will increase the magnetic field in the aperture. It may also deteriorate the field quality even for a large-aperture magnet. Detailed finite-element analysis will be required to clarify both aspects.

Although the CCT design offers excellent geometric field quality as shown in Tables III and V, these field error values are computed without considering the magnet fabrication and assembly tolerance that can lead to field errors. In addition, the persistent magnetization in superconductors and dynamic effects cause additional field errors in CCT magnets [28], [66], [67]. A higher critical current in CORC® wires can exacerbate the issue but promising mitigation methods exist [10], [68].

For the results reported here, the tilt angle of each layer (Section III) is chosen such that the minimum bend radius of the winding is or approaches 30 mm, the minimum bend

radius of CORC®-02 wire. For a magnet aperture of 150 mm, these tilt angles are sufficiently low for a high efficiency in field generation. On the other hand, small tilt angles elongate the coil ends, which can consume more conductors for a short magnet (Table II). More detailed study is required on the trade-off between the magnet efficiency and conductor usage [53].

Conductor grading is not considered for the wire length presented in Tables II and IV. The averaged conductor-field load line in Layer 6 is 62% of that in Layer 1 for the six-layer three-wire design (Fig. 2). Therefore, there is room for grading and conductor saving. One may grade the CORC® wire using fewer tapes or using tapes with lower I_c.

Model coils using prototype conductors should be built and tested to determine the feasibility of a magnet concept. The community will also benefit from investigating diverse magnet concepts and conductor architectures. The Conductor on Molded Barrel design, under investigation at Fermi National Accelerator Laboratory [27], can offer effective stress management and efficient conductor usage. Nes and collaborators designed a cloverleaf-type dipole magnet using dual-REBCO tape conductor to generate a dipole field of 9.4 T [69]. We need to be creative to secure expensive yet much-needed conductors.

Testing magnets with relevant magnetic fields in relevant conditions can also help develop quench detection and protection technology [70] that is critical for REBCO magnets with high stored energy (Tables II and IV). Detailed analysis on the quench protection should be developed and validated against the experimental data.

Of particular interest is to test REBCO magnets in liquid H_2. Not only the impact on the magnet stability and field quality is worth studying but also we can get familiar again with liquid H_2 as a coolant [71], [72]. Although we sacrifice significant magnetic-field performance from 4.2 K, what we will learn can help improve the sustainability of future energy-frontier colliders.

V. Conclusions

High-temperature superconducting REBCO magnets can generate high magnetic fields beyond liquid helium temperature. This potential can make future machines such as a muon collider more affordable and sustainable.

We present an initial scoping study with magnet designs that can generate a dipole field of 8 – 10 T in a REBCO magnet with an aperture of 150 mm. The study is based on the canted $\cos\theta$ (CCT) concept, without iron. The conceptual magnets consist of up to six layers, using a ribbon-type cable of up to three CORC® wires in each layer. Based on the performance of existing CORC® wires, the dipole case can generate 13.2 T, the short-sample prediction at 4.2 K and 8.9 T at 20 K. The 33% reduction in dipole field at 20 K is due to the reduced current-carrying capability in REBCO conductors at higher temperatures. A combined-function case can generate a dipole field of 8 T with a gradient of about 50 T m^{-1} at 4.2 K, partially meeting the requirements of a lattice design for a muon collider with a center-of-mass of 3 TeV.

The magnets have an outer diameter of 370 mm without iron. Without conductor grading, about 2.3 km long CORC® wires or 130 km long REBCO tapes would be required for a six-layer three-wire dipole-magnet design with a 1 m long magnetic length. We need to continue engaging and collaborating with conductor vendors to increase the critical current of REBCO conductors.

The results reported here and follow-up studies will help develop the REBCO magnet and conductor technology to meet the needs of future energy-frontier colliders.

Acknowledgment

We thank Luca Bottura of CERN and Samuele Mariotto of University of Milan for the discussions on the magnet needs in the storage ring of a muon collider and the potential of HTS magnets to meet the needs. We thank Anis Ben Yahia, Ramesh Gupta and Mithlesh Kumar of Brookhaven National Laboratory, Vadim Kashihkin and Vito Lombardo of Fermi National Accelerator Laboratory, and Sofia Viarengo of Politecnico di Torino for the discussions on REBCO magnet technology development. We also thank Michael Benedikt, Serge Claudet and Frank Zimmermann of CERN for the discussions on the cooling efficiency at cryogenic temperatures. We thank Jean-François Croteau of Lawrence Berkeley National Laboratory for suggesting the references on liquid hydrogen. Last but not least, we thank Al Zeller of the National High Magnetic Field Laboratory for his support of the study and resulting manuscript.

Appendix A
Impact of Operating Temperature on the Performance of REBCO Magnets

Suppose the critical current of the conductor follows a power law, such as (1), at different temperatures. When a magnet is iron free, the peak field on the conductor scales linearly with the current, $I = \gamma B$, where γ is a constant. The conductor peak field at the short-sample limit is

$$B = \left(\frac{\gamma}{\beta}\right)^{\frac{1}{\alpha-1}}, \tag{6}$$

where α and β are defined in (1).

The ratio between the peak conductor fields at temperatures T_1 and T_2 is then

$$\frac{B(T_1)}{B(T_2)} = \left(\frac{\gamma}{\beta(T_1)}\right)^{\frac{1}{\alpha(T_1)-1}} \left(\frac{\beta(T_2)}{\gamma}\right)^{\frac{1}{\alpha(T_2)-1}}. \tag{7}$$

If the exponents α are similar at both temperatures, then the ratio becomes

$$\frac{B(T_1)}{B(T_2)} = \left(\frac{\beta(T_2)}{\beta(T_1)}\right)^{\frac{1}{\alpha-1}}. \tag{8}$$

Equation (8) explains why, without the iron, the magnet performance at 20 K is about 33% lower than that at 4.2 K, given $\beta(20\text{ K})/\beta(4.2\text{ K}) = 0.5$ and $\alpha = -0.77$.

REFERENCES

[1] L. Bottura, S. Prestemon, L. Rossi *et al.*, "Superconducting magnets and technologies for future colliders," *Frontiers in Physics*, vol. 10, 2022.

[2] R. B. Palmer, "Muon colliders," *Reviews of Accelerator Science and Technology*, vol. 07, pp. 137–159, Jan. 2014.

[3] M. Boscolo, J.-P. Delahaye, and M. Palmer, "The future prospects of muon colliders and neutrino factories," *Reviews of Accelerator Science and Technology*, vol. 10, no. 01, pp. 189–214, Aug. 2019.

[4] K. R. Long, D. Lucchesi, M. A. Palmer *et al.*, "Muon colliders to expand frontiers of particle physics," *Nature physics*, vol. 17, no. 3, pp. 289–292, Jan. 2021.

[5] D. Schulte, M. Palmer, T. Arndt *et al.*, *European Strategy for Particle Physics — Accelerator R&D Roadmap*, 2022, ch. Bright Muon Beams and Muon Colliders, pp. 147–185.

[6] M. Narain, L. Reina, A. Tricoli *et al.*, "The future of US particle physics – the Snowmass 2021 energy frontier report," https://arxiv.org/abs/2211.11084, Nov. 2022.

[7] E. Todesco, L. Bottura, G. de Rijk *et al.*, "Dipoles for high-energy LHC," *IEEE Trans. Appl. Supercond.*, vol. 24, no. 3, p. 4004306, June 2014.

[8] S. Prestemon, K. Amm, L. Cooley *et al.*, "The 2020 updated roadmaps for the US Magnet Development Program," http://arxiv.org/abs/2011.09539, Oct. 2020.

[9] P. Ferracin, G. Ambrosio, D. Arbelaez *et al.*, "Towards 20 T hybrid accelerator dipole magnets," *IEEE Trans. Appl. Supercond.*, vol. 32, no. 6, p. 4000906, Sep. 2022.

[10] J. van Nugteren, G. Kirby, J. Murtomäki *et al.*, "Toward REBCO 20 T+ dipoles for accelerators," *IEEE Trans. Appl. Supercond.*, vol. 28, no. 4, p. 4008509, June 2018.

[11] P. Ferracin and E. Rochepault, "Design limits for accelerator dipoles and quadrupoles," https://indico.cern.ch/event/1175126/contributions/5024314/, October 2022.

[12] D. C. Larbalestier, J. Jiang, U. P. Trociewitz *et al.*, "Isotropic round-wire multifilament cuprate superconductor for generation of magnetic fields above 30 T," *Nature materials*, vol. 13, no. 4, pp. 375–381, Apr. 2014.

[13] S. Claudet, G. Ferlin, F. Millet *et al.*, "1.8 K refrigeration units for the LHC: Performance assessment of pre-series units," in *Proceedings of the Twentieth International Cryogenic Engineering Conference (ICEC20)*, L. Zhang, L. Lin, and G. Chen, Eds. Oxford: Elsevier Science, 2005, pp. 999–1002. [Online]. Available: https://doi.org/10.1016/B978-008044559-5/50239-8

[14] H. Gruehagen and U. Wagner, "Measured performance of four new 18 kW@4.5 K helium refrigerators for the LHC cryogenic system," in *Proceedings of the Twentieth International Cryogenic Engineering Conference (ICEC20)*, L. Zhang, L. Lin, and G. Chen, Eds. Elsevier Science, 2005, pp. 991–994. [Online]. Available: https://doi.org/10.1016/B978-008044559-5/50237-4

[15] D. Stratakis, N. Mokhov, M. Palmer *et al.*, "A muon collider facility for physics discovery," https://arxiv.org/abs/2203.08033, Mar. 2022.

[16] B. Owens, "Energy crisis squeezes science at CERN and other major facilities," *Nature*, vol. 610, no. 7932, pp. 431–432, Oct. 2022.

[17] M. Giovannozzi, M. Benedikt, A. Chance *et al.*, "Status and challenges of the future circular hadron collider FCC-hh," in *Proceedings of 41st International Conference on High Energy physics — PoS(ICHEP2022)*. Trieste, Italy: Sissa Medialab, Nov. 2022.

[18] C. M. Ankenbrandt, M. Atac, B. Autin *et al.*, "Status of muon collider research and development and future plans," *Physical Review Special Topics - Accelerators And Beams*, vol. 2, p. 081001, 1999.

[19] A. F. Zeller, V. Blideanu, R. M. Ronningen *et al.*, "Radiation resistant magnets for the RIA fragment separator," in *Proceedings of the 2005 Particle Accelerator Conference*, May 2005, pp. 2200–2202.

[20] R. Gupta, M. Anerella, J. Cozzolino *et al.*, "HTS quadrupole for FRIB–design, construction and test results," *IEEE Trans. Appl. Supercond.*, vol. 25, no. 3, p. 4603306, 2015.

[21] W. P. Halperin, "The impact of helium shortages on basic research," *Nature physics*, vol. 10, no. 7, pp. 467–470, Jun. 2014.

[22] M. Durante, F. Borgnolutti, D. Bouziat *et al.*, "Realization and first test results of the EuCARD 5.4-T REBCO dipole magnet," *IEEE Trans. Appl. Supercond.*, vol. 28, no. 3, p. 4203805, April 2018.

[23] J. van Nugteren, G. Kirby, H. Bajas *et al.*, "Powering of an HTS dipole insert-magnet operated standalone in helium gas between 5 and 85 K," *Superconductor Science and Technology*, vol. 31, no. 6, p. 065002, April 2018.

[24] L. Rossi and C. Senatore, "HTS accelerator magnet and conductor development in Europe," *Instruments*, vol. 5, no. 1, p. 8, Feb. 2021, and references therein.

[25] S. A. Gourlay, S. O. Prestemon, A. V. Zlobin *et al.*, "The U.S. Magnet Development Program plan," https://escholarship.org/uc/item/5178744r, June 2016.

[26] R. Gupta, "New approach and test facility for high field accelerator magnets R&D," https://www.bnl.gov/magnets/staff/gupta/publications/mt26/wed-af-or13-02-submit-201 2019.

[27] V. Kashikhin, V. Lombardo, and G. Velev, "Magnet design optimization for future hadron colliders." JACOW Publishing, Geneva, Switzerland, Jun. 2019, pp. 4307–4310, https://doi.org/10.18429/JACoW-IPAC2019-THPTS084.

[28] X. Wang, D. Abraimov, D. Arbelaez *et al.*, "Development and performance of a 2.9 Tesla dipole magnet using high-temperature superconducting CORC® wires," *Superconductor Science and Technology*, vol. 34, no. 1, p. 015012, Dec. 2020.

[29] X. Wang, T. J. Bogdanof, P. Ferracin *et al.*, "An initial magnet experiment using high-temperature superconducting STAR® wires," *Superconductor Science and Technology*, vol. 35, no. 12, p. 125011, Nov. 2022.

[30] L. Bromberg, M. Tekula, L. A. El-Guebaly *et al.*, "Options for the use of high temperature superconductor in tokamak fusion reactor designs," *Fusion Engineering and Design*, vol. 54, no. 2, pp. 167–180, Feb. 2001.

[31] Z. S. Hartwig, C. B. Haakonsen, R. T. Mumgaard *et al.*, "An initial study of demountable high-temperature superconducting toroidal field magnets for the vulcan tokamak conceptual design," *Fusion Engineering and Design*, vol. 87, no. 3, pp. 201–214, Mar. 2012.

[32] B. Sorbom, J. Ball, T. Palmer *et al.*, "ARC: A compact, high-field, fusion nuclear science facility and demonstration power plant with demountable magnets," *Fusion Engineering and Design*, vol. 100, pp. 378–405, 2015.

[33] D. G. Whyte, J. Minervini, B. LaBombard *et al.*, "Smaller & sooner: exploiting high magnetic fields from new superconductors for a more attractive fusion energy development path," *J. Fusion Energy*, vol. 35, no. 1, pp. 41–53, February 2016.

[34] X. Wang, A. Ben Yahia, E. Bosque *et al.*, "REBCO – a silver bullet for our next high-field magnet and collider budget?" https://arxiv.org/abs/2203.08736, Mar. 2022.

[35] Y. Alexahin, E. Gianfelice-Wendt, and V. Kapin, "Muon collider lattice concepts," *Journal of Instrumentation*, vol. 13, no. 11, p. P11002, Nov. 2018.

[36] A. V. Zlobin, Y. I. Alexahin, V. V. Kashikhin *et al.*, "Magnet designs for muon collider ring and interactions regions," in *Proceedings of IPAC 2010*, 2010, pp. 388–390.

[37] I. Novitski, V. V. Kashikhin, N. Mokhov *et al.*, "Conceptual designs of dipole magnet for muon collider storage ring," *IEEE Trans. Appl. Supercond.*, vol. 21, no. 3, pp. 1825–1828, Jun. 2011.

[38] V. V. Kashikhin, Y. I. Alexahin, N. V. Mokhov *et al.*, "High-field combined-function magnets for a 1.5×1.5 TeV muon collider storage ring," in *Proceedings of IPAC2012*. IEEE-NPSS, 2012, pp. 3587–3589.

[39] M. L. Lopes, V. Kashikhin, J. C. Tompkins *et al.*, "Design studies of a dipole with elliptical aperture for the muon collider storage ring," in *Proceedings of IPAC2012*. IEEE-NPSS, 2012, pp. 3590–3592.

[40] N. V. Mokhov, V. V. Kashikhin, S. I. Striganov *et al.*, "The higgs factory muon collider superconducting magnets and their protection against beam decay radiation," *Journal of Instrumentation*, vol. 13, no. 10, p. P10024, Oct. 2018.

[41] D. C. van der Laan, "$YBa_2Cu_3O_{7-\delta}$ coated conductor cabling for low ac-loss and high-field magnet applications," *Superconductor Science and Technology*, vol. 22, no. 6, p. 065013, 2009.

[42] J. D. Weiss, T. Mulder, H. J. ten Kate *et al.*, "Introduction of CORC® wires: highly flexible, round high-temperature superconducting wires for magnet and power transmission applications," *Superconductor Science and Technology*, vol. 30, no. 1, p. 014002, 2017, and references therein.

[43] J. D. Weiss, D. C. van der Laan, D. Hazelton *et al.*, "Introduction of the next generation of CORC® wires with engineering current density exceeding 650 A mm^{-2} at 12 T based on SuperPower's ReBCO tapes containing substrates of 25 μm thickness," *Superconductor Science and Technology*, vol. 33, no. 4, p. 044001, Feb. 2020.

[44] C. Senatore, C. Barth, M. Bonura *et al.*, "Field and temperature scaling of the critical current density in commercial REBCO coated conductors," *Superconductor Science and Technology*, vol. 29, no. 1, p. 014002, Dec. 2015.

[45] A. Molodyk, S. Samoilenkov, A. Markelov *et al.*, "Development and large volume production of extremely high current density $YBa_2Cu_3O_7$ superconducting wires for fusion," *Scientific reports*, vol. 11, no. 1, p. 2084, Jan. 2021.

[46] SuperPower Inc., "2G HTS wire specification," https://www.superpower-inc.com/specification.aspx, (accessed on 20 November 2022).

[47] J. Barber, J. Brisson, and J. Minervini, "Forced flow cooling of high field, REBCO-based, fusion magnets using supercritical hydrogen, helium, and neon," *Cryogenics*, vol. 96, pp. 34–43, Dec. 2018.

[48] D. Meyer and R. Flasck, "A new configuration for a dipole magnet for use in high energy physics applications," *Nuclear Instruments and Methods*, vol. 80, no. 2, pp. 339–341, 1970.

[49] A. V. Gavrilin, M. D. Bird, S. T. Bole *et al.*, "Conceptual design of high transverse field magnets at the NHMFL," *IEEE Trans. Appl. Supercond.*, vol. 12, no. 1, pp. 465–469, March 2002.

[50] A. Devred, "High field accelerator magnets beyond LHC," in *Proceedings of Particle Accelerator Conference*, 2003.

[51] C. L. Goodzeit, M. J. Ball, and R. B. Meinke, "The double-helix dipole — a novel approach to accelerator magnet design," *IEEE Trans. Appl. Supercond.*, vol. 13, no. 2, pp. 1365–1368, June 2003.

[52] S. Caspi, F. Borgnolutti, L. Brouwer *et al.*, "Canted-cosine-theta magnet (CCT) — a concept for high field accelerator magnets," *IEEE Trans. Appl. Supercond.*, vol. 24, no. 3, p. 4001804, June 2014, and references therein.

[53] L. N. Brouwer, "Canted-cosine-theta superconducting accelerator magnets for high energy physics and ion beam cancer therapy," Ph.D. dissertation, University of California, Berkeley, 2015, https://escholarship.org/uc/item/8jp4g75g.

[54] L. Quéval and R. Gottkehaskamp, "Analytical field calculation of modulated double helical coils," *IEEE Transactions on Applied Superconductivity*, vol. 25, no. 6, p. 4901307, Dec. 2015.

[55] S. Farinon and R. Musenich, "Biot–Savart approach to analytical computation of magnetic fields and forces of CCT magnets," *IEEE Trans. Appl. Supercond.*, vol. 31, no. 3, p. 4900308, Apr. 2021.

[56] G. Majkic, Y. Yao, J. Liu *et al.*, "Effect of high BZO dopant levels on performance of 2G-HTS MOCVD wire at intermediate and low temperatures," *IEEE Trans. Appl. Supercond.*, vol. 23, no. 3, p. 6602605, Jun. 2013.

[57] T. Nakamoto, N. Higashi, T. Ogitsu *et al.*, "Design of superconducting combined function magnets for the 50 GeV proton beam line for the J-PARC neutrino experiment," *IEEE Trans. Appl. Supercond.*, vol. 14, no. 2, pp. 616–619, Jun. 2004.

[58] T. Ogitsu, Y. Ajima, M. Anerella *et al.*, "Superconducting combined function magnet system for J-PARC neutrino experiment," *IEEE Trans. Appl. Supercond.*, vol. 15, no. 2, pp. 1175–1180, Jun. 2005.

[59] C. Goodzeit, R. Meinke, and M. Ball, "Combined function magnets using double-helix coils," in *Proceedings of PAC07*, Jun. 2007, pp. 560–562.

[60] S. Caspi, D. Arbelaez, H. Felice *et al.*, "Conceptual design of a 260 mm bore 5 T superconducting curved dipole magnet for a carbon beam therapy gantry," *IEEE Trans. Appl. Supercond.*, vol. 22, no. 3, p. 4401204, Jun. 2012.

[61] D. C. van der Laan, J. D. Weiss, and D. M. McRae, "Status of CORC® cables and wires for use in high-field magnets and power systems a decade after their introduction," *Superconductor Science and Technology*, vol. 32, no. 3, p. 033001, February 2019, and references therein.

[62] D. C. van der Laan, D. M. McRae, and J. D. Weiss, "Effect of transverse compressive monotonic and cyclic loading on the performance of superconducting CORC® cables and wires," *Superconductor Science and Technology*, vol. 32, no. 1, p. 015002, November 2018.

[63] L. Brouwer, D. Arbelaez, S. Caspi *et al.*, "Improved modeling of Canted–Cosine–Theta magnets," *IEEE Trans. Appl. Supercond.*, vol. 28, no. 3, p. 4001006, Apr. 2018.

[64] L. Brouwer, M. Juchno, D. Arbelaez *et al.*, "Design of CCT6: A large aperture, Nb_3Sn dipole magnet for HTS insert testing," *IEEE Trans. Appl. Supercond.*, vol. 32, no. 6, p. 4001805, Sep. 2022.

[65] E. Todesco, "Masterclass — design of superconducting magnets for particle accelerators. Unit 9, iron effect and grading design," https://indico.cern.ch/event/925561/attachments/2065861/3467216/9.pdf, Jun. 2020, accessed: 2022-11-21.

[66] S. Caspi, L. N. Brouwer, T. Lipton *et al.*, "Test results of CCT1—a 2.4 T canted-cosine-theta dipole magnet," *IEEE Trans. Appl. Supercond.*, vol. 25, no. 3, p. 4002304, June 2015.

[67] X. Wang, D. R. Dietderich, J. DiMarco *et al.*, "A 1.2 T canted $\cos\vartheta$ dipole magnet using high-temperature superconducting CORC® wires," *Superconductor Science and Technology*, vol. 32, no. 7, p. 075002, May 2019.

[68] L. Bortot, M. Mentink, C. Petrone *et al.*, "High-temperature superconducting screens for magnetic field-error cancellation in accelerator magnets," *Superconductor Science and Technology*, vol. 34, no. 10, p. 105001, Aug. 2021.

[69] T. H. Nes, G. Kirby, G. de Rijk *et al.*, "Design of a cloverleaf-racetrack dipole demonstrator magnet with dual ReBCO conductor," *IEEE Trans. Appl. Supercond.*, vol. 32, no. 6, p. 4002105, Sep. 2022.

[70] M. Marchevsky, "Quench detection and protection for high-temperature superconductor accelerator magnets," *Instruments*, vol. 5, no. 3, p. 27, Aug. 2021, and references therein.

[71] H. L. Laquer and E. F. Hammel, "Cryogenic electromagnets. i. feasibility study," *The Review of scientific instruments*, vol. 28, no. 11, pp. 875–878, Nov. 1957.

[72] Y. Iwasa, "Liquid hydrogen condenser and current lead designs for liquid hydrogen critical current measurements of superconductors," *Cryogenics*, vol. 31, no. 3, pp. 174–177, Mar. 1991.